Pis'ma v ZhETF, vol. 84, iss. 10, pp. 666 – 672

Spin photocurrents and circular photon drag effect in (110)-grown quantum well structures

V. A. Shalygin[1)], *H. Diehl*[+], *Ch. Hoffmann*[+], *S. N. Danilov*[+], *T. Herrle*[+], *S. A. Tarasenko*[*], *D. Schuh*[+], *Ch. Gerl*[+], *W. Wegscheider*[+], *W. Prettl*[+], *S. D. Ganichev*[+]

St. Petersburg State Polytechnic University, 195251 St. Petersburg, Russia

[+]*Fakulty Physics, University of Regensburg, 93040 Regensburg, Germany*

[*] *A.F. Ioffe Physico-Technical Institute RAS, 194021 St. Petersburg, Russia*

Submitted 26 October 2006

We report on the study of spin photocurrents in (110)-grown quantum well structures. Investigated effects comprise the circular photogalvanic effect and so far not observed circular photon drag effect. The experimental data can be described by an analytical expression derived from a phenomenological theory. A microscopic model of the circular photon drag effect is developed demonstrating that the generated current has spin dependent origin.

PACS: 72.25.Fe, 72.25.Rb, 73.50.Pz, 78.67.De

1. Introduction. There is a growing interest in the field of spintronics with the aim of controlling and manipulating electron spins in microelectronic devices. A key factor for semiconductor spintronics is spin relaxation time: it must be sufficiently long for the processing of information encoded as spin polarization. In the case of a two-dimensional semiconductor structure spin relaxation time strongly depends on the growth direction. It was shown that in (110)-grown GaAs/AlGaAs quantum wells (QWs) spin relaxation time is considerably longer compared to that in (001)-oriented QWs and, therefore, it can be increased to nanoseconds even at room temperature [1]. This is due to the fact that in (110)-grown QWs the D'yakonov-Perel' mechanism of spin relaxation dominating in GaAs heterostructures is suppressed. This observation has attracted a great deal of attention to spin dependent phenomena in (110)-oriented structures. An effective access to these phenomena in low dimensional structures is provided by spin photocurrents like circular photogalvanic effect (CPGE) [2 – 4] and spin-galvanic effect (SGE) [5], allowing investigation of spin relaxation times, spin splitting of the band structure, symmetry properties, etc. (for a review see [6, 7]). So far spin photocurrents were mostly studied in (001)- and (113)-grown heterostructures.

In this letter we present investigations of the circular photogalvanic effect in n-type (110)-grown GaAs/AlGaAs QWs and report on the observation of a new effect caused by transfer of both linear and angular momenta of photons to free carriers. The latter effect, called circular photon drag effect, was theoretically predicted in Refs. [8, 9], but so far not observed. All previous investigations dealt with the linear photon drag effect where the inversion of the light helicity does not affect the sign and magnitude of the current (for review see [6, 10, 11]). The circular photon drag effect reported here, in contrast, represents the photon drag current which reverses its direction by inversion of the light helicity from left-handed to right-handed and vice versa.

2. Experimental technique. The experiments are carried out at room temperature on asymmetrical (110)-oriented GaAs/Al_xGa_{1-x}As molecular beam epitaxy grown heterostructures containing 100 QWs of 8.2 nm width separated by 40 nm barriers ($x = 0.34$). Two n-type structures with electron concentration n_s about $7 \cdot 10^{11}\,\text{cm}^{-2}$ per QW and various doping profiles are investigated. The sample A contains Si-doped layer of 10 nm width in each barrier shifted from the barrier center by the distance of 10 nm. In sample B the doped layer of the same width is placed in the center of each barrier. Samples have sizes about $5 \times 5\,\text{mm}^2$. The sample edges are oriented along $x \parallel [1\bar{1}0]$ and $y \parallel [00\bar{1}]$ in the QW plane, the z-axis points parallel to the structure growth direction. To measure electrical currents ohmic contacts are prepared in the center of each sample edge.

The measurements of photocurrents are carried out under excitation of the samples with infrared or terahertz radiation at normal and oblique incidence. The source of infrared radiation is a Q-switch CO_2-laser with operating spectral range (9.2–10.8 μm) corresponding to *inter*-subband transitions between the lowest and the

[1)]e-mail: shalygin@rphf.spbstu.ru

first excited subbands of the investigated QWs. Pulsed THz radiation is obtained applying an optically pumped pulsed molecular laser [6]. Several wavelengths between 77 and 496 μm have been selected using NH_3, D_2O and CH_3F as active media. Terahertz radiation causes the *intra*-subband (Drude-like) absorption of the radiation. The geometry of the experiment is sketched in the inset of Fig.1b. The photocurrent is measured in unbiased structures via the voltage drop across a 50 Ω load resistor.

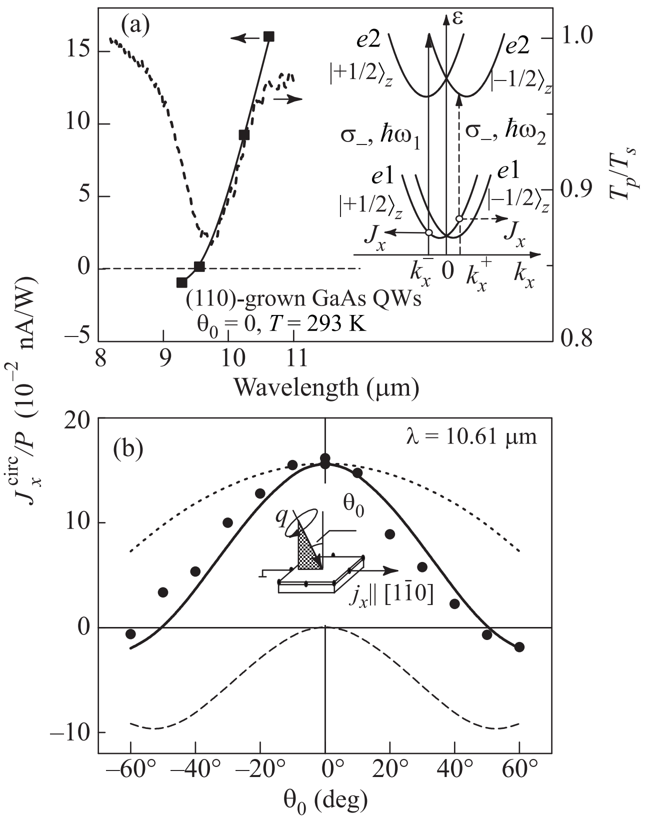

Fig.1. (a) Spectrum of helicity dependent photocurrent $J_x^{\rm circ}$ normalized to the laser power P measured in sample A illuminated by infrared laser radiation under normal incidence (squares) and spectrum of optical transmission ratio T_p/T_s (dashed line) for light of p- and s-polarization, respectively. Solid line is a guide for the eye. The transmission spectrum is measured under oblique incidence at $\theta_0 = 60°$. The inset shows the model of the circular photogalvanic effect caused by direct intersubband transitions and illustrates the spectral inversion of the photocurrent induced by σ_- radiation due to reduction of the photon energy from $\hbar\omega_1$ to $\hbar\omega_2$. (b) Angular dependence of normalized helicity dependent photocurrent $J_x^{\rm circ}/P$ obtained for sample A. The doted, dashed, and solid curves are fit after Eq. (4) and represent, correspondingly, the term in square brackets, the last term on the right hand side of Eq. (4), and the sum of both terms. The inset shows the experimental geometry

In this work we examine helicity dependent photocurrents, $J_x^{\rm circ}$, i.e. currents which reverse their sign upon switching the radiation helicity. In order to extract such a current contribution from the measured total current we determined the response to σ_+ and σ_- radiation and evaluated the data after

$$J_x^{\rm circ} = [J_x(\sigma_+) - J_x(\sigma_-)]/2\,. \qquad (1)$$

The right-handed (σ_+) and left-handed (σ_-) circularly polarized radiation is achieved by means of a Fresnel rhomb in the infrared and λ-quarter quartz plates in the THz range.

3. Experimental results and discussion. Irradiating the samples at normal incidence we detected a photocurrent which is proportional to the radiation helicity $P_{\rm circ}$ and whose temporal structure reproduces that of the laser pulse being of the order of 100 ns. This helicity dependent current has been observed with the contact pairs aligned along $x \parallel [1\bar{1}0]$ only. All these features hold for infrared as well as THz wavelengths applied and are in agreement with phenomenological theory. In fact, asymmetric (110)-oriented heterostructures used in our experiments belong to media of C_s point-group symmetry. In this symmetry the circular photocurrent density j_x excited by light incident in the xz plane is given by

$$j_x = \gamma_{xz}\, t_p t_s \frac{q_z}{q} {E_0}^2 P_{\rm circ}, \qquad (2)$$

where $\boldsymbol{\gamma}$ is the second rank pseudo-tensor describing the sum of the circular photogalvanic effect [2] and optical orientation induced spin-galvanic effect [5], t_p and t_s are the transmission coefficients for p and s components of the light electric field, $\mathbf{q}$ is the light wave vector inside the medium, E_0 is the electric field amplitude of the incident light, and $P_{\rm circ}$ is the light helicity ($P_{circ} = \pm 1$ for $\sigma_\pm$ polarization, respectively). The difference of the currents for $P_{circ} = \pm 1$ yields j_x^{circ}. The dependence of the photocurrent on the angle of incidence θ_0 is given by $q_z/q = \cos\theta$ and Fresnel's formulas for t_p and t_s,

$$t_p t_s = \frac{4\cos^2\theta_0}{(\cos\theta_0 + n_\omega \cos\theta)(n_\omega\cos\theta_0 + \cos\theta)}\,,$$

where θ is the angle of refraction defined by $\sin\theta = \sin\theta_0/n_\omega$ and n_ω is the refraction index of the medium.

Measurements of spectral behavior of $J_x^{\rm circ}$ in the infrared range show a spectral inversion as plotted in Fig.1a. The point of the inversion corresponds to the maximum of resonant intersubband absorption which is measured by means of the Fourier transform transmission spectroscopy. The fact that the photocurrent changes sign by tuning the wavelength indicates that it is mainly caused by the CPGE outweighing the spin-galvanic effect [12]. The model picture of the CPGE illustrating the spectral sign inversion of the current at the center of the absorption line is sketched in the inset of Fig.1a after [13]. In structures of C_s symmetry the spin-orbit coupling splits the electron spectrum into spin branches with the spin components $s_z = \pm 1/2$ along the growth direction. The relevant contribution to spin-orbit part of the effective Hamiltonian is given by $\beta_{zx}\sigma_z k_x$, where β_{zx} is a parameter and σ_z is the Pauli matrix. Due to the optical selection rules, the normaly-incident circularly polarized radiation, e.g. σ_-, induces direct optical transitions from the subband $e1$ with the spin $s_z = +1/2$ to the subband $e2$ with $s_z = -1/2$. Monochromatic radiation with the certain photon energy, say $\hbar\omega_1$, induces the transitions only at a fixed wave vector k_x^- where the photon energy matches the transition energy as indicated by the solid vertical arrow in the inset of Fig.1a. Thus, the intersubband excitation results in an imbalance of the momentum distribution between positive and negative k_x in both subbands yielding an electric current. As in our QWs the energy separation between the subbands ε_{21} is larger than the energy of longitudinal optical phonons ($\varepsilon_{21} \approx 100$ meV, $\hbar\Omega_{\text{LO}} = 35$ meV), the nonequilibrium distribution of electrons in the subband $e2$ relaxes rapidly due to the emission of phonons. By that the contribution of the subband $e2$ to the electric current vanishes. Therefore, the magnitude and the direction of the current, shown in the inset of Fig.1a by the solid horizontal arrow, is determined by the group velocity and the momentum relaxation time τ_{e1} of the photogenerated "holes" in the subband $e1$ with $s_z = +1/2$. Obviously, the whole picture mirrors and the current direction reverses by switching the circular polarization from left- to right-handed. Spectral inversion of the photocurrent at fixed helicity also follows from this model picture. Indeed, as is shown in Fig.1a, decreasing the photon frequency to $\hbar\omega_2$ shifts the transitions toward positive k_x (dashed vertical arrow), and the direction of the current reverses (dashed horizontal arrow). The inversion of the current direction takes place at the photon energy corresponding to the optical transitions from the spin subband minima. This mechanism is based on spin splitting due to $\sigma_z k_x$ terms and predicts, in accordance with the phenomenological equation (2), that the current reaches a maximum at normal incidence and becomes smaller under oblique incidence keeping the same direction.

In order to cross-check the validity of the phenomenological Eq. (2) with respect to our measurements, we investigated the current response as a function of the incidence angle θ_0. In the whole THz range, where the photocurrent is caused by Drude absorption, we found that the data are well described by this equation. However, in the infrared range a qualitative discrepancy to Eq. (2) is observed. In contrast to the sign conserving behavior of the photocurrent given by $t_p t_s \cos\theta$, the signal in the sample A changes its sign twice at $\theta_0 \approx \pm 50°$, see Fig.1b. The experiment carried out on the sample B gave the effect even more pronounced: here the inversion takes place at $\theta_0 \approx \pm 30°$, see inset of Fig.2. We note

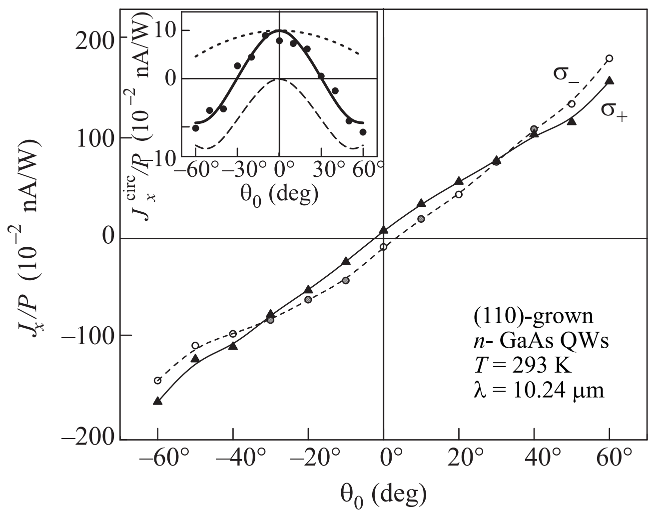

Fig.2. Dependencies of the total photocurrent J_x normalized to the laser power P on the angle of incidence θ_0 obtained for sample B illuminated with right-handed (σ_+, triangles) and left-handed (σ_-, circles) circularly polarized radiation. Lines are a guide for the eye. The inset shows the angular dependence of the helicity dependent part of the normalized photocurrent, J_x^{circ}/P, for the same structure. The doted, dashed, and solid curves are fit after Eq. (4) and represent, correspondingly, the term in square brackets, the last term on the right hand side of Eq. (4), and the sum of both terms

that in contrast to normal incidence of radiation, where only helicity dependent current is observed, at oblique incidence a substantial helicity independent contribution to the total current is found, see Fig.2. This contribution is due to the linear photogalvanic effect [14, 15] and the linear photon drag effect [16, 17], which are out of scope of this letter. Nevertheless, the helicity dependent contribution J_x^{circ} is large enough and is easily measurable. In particular, the twofold sign inversion of the helicity dependent photocurrent with incidence angle variation is clearly seen in Fig.2.

This angle inversion of the current direction cannot be explained in the framework of the conventional theory of the CPGE or optically excited SGE which ignores the linear momentum transfer from photons to free carriers. Taking into account the linear momentum of the photon, neglected in Eq. (2), we obtain an additional contribution to the current excited by circularly polarized light. Then, the total helicity dependent photocurrent in structures of C_s symmetry is given by

$$j_x = t_p t_s \left\{ \left[(\gamma_{xz} + q_z T_{xzz}) \frac{q_z}{q} \right] + q_x T_{xxx} \frac{q_x}{q} \right\} E_0{}^2 P_{\text{circ}}, \quad (3)$$

where $\mathbf{T}$ is the third rank tensor which describes the circular photon drag effect. Following Eq. (3) one obtains the angular dependence of the photocurrent

$$j_x = t_p t_s \{ [(\gamma_{xz} + q T_{xzz} \cos\theta) \cos\theta] + + q T_{xxx} \sin^2\theta \} E_0{}^2 P_{circ}. \quad (4)$$

Equation (4) shows that the circular photon drag effect given by terms containing the linear photon momentum $\mathbf{q}$ can be observed, in principle, at both normal ($\theta = 0$) and oblique incidence. However, distinction between contributions of the CPGE and of the circular photon drag effect for $\theta = 0$ is not an easy task. It may be done keeping in mind that the replacement $P_{circ} \to -P_{circ}$ and $q_z \to -q_z$ in Eq. (3) conserves the first term in the square brackets on the right hand side of Eq. (3) while changes the sign of the second term. Experimentally it can be realized putting a mirror behind the sample and comparing the current magnitudes with and without mirror. However, such a method requires very high accuracy of adjustment.

Much more reliable access to the circular photon drag effect is provided by studying the angular dependence of the photocurrent. Indeed, the terms in square brackets in Eq. (4) have a maximum at normal incidence and their contribution to the current decreases with increasing the angle of incidence. At the same time the circular photon drag effect given by the last term in Eq. (4) vanishes at normal incidence and increases with $|\theta_0|$. This interplay of the current contributions may result in the observed twofold sign inversion of the total current by the variation of θ_0 from $-\pi/2$ to $\pi/2$ if the circular photon drag and the CPGE photocurrents are oppositely directed. The fits of Eq. (4) to the experimental data for both QW structures are shown in Fig.1b and in the inset of Fig.2. The plotted curves represent the terms in square brackets (doted curves), the last term on the right hand side of Eq. (4) (dashed curves), and the sum of both terms (solid curves). To fit the data for each sample we use an ordinate scaling parameter for the doted curve to obtain agreement at normal incidence, where the last term on the right hand side of Eq. (4) vanishes. Then, the dashed curve is scaled to fit the data in the whole range of the incidence angles θ_0. It is seen that the phenomenological equation (4) describes well the experimental angular dependence of the photocurrent. The contribution to the circular photon drag effect given by the component T_{xxx} reaches its maximum in GaAs/AlGaAs structures at $\theta_0 \approx \pm 50°$.

4. Microscopical model. Now we discuss the microscopic picture of the observed circular photon drag effect given by the last term on the right hand side of Eq. (3). The tensor $\mathbf{T}$ is not invariant under time inversion. Therefore, dissipative processes should be involved in the microscopic model of the effect. The proposed model includes three stages.

The first stage is a helicity and photon wave vector dependent photoexcitation. The intersubband absorption of circularly polarized radiation is a spin dependent process. While at normal incidence the absorption of circularly polarized light is due to spin-flip processes (see inset in Fig.1a), under oblique excitation due to selection rules the absorption is dominated by spin conserving transitions [18]. However, the rates of these spin conserving transitions are different for electrons with the spin oriented parallel and antiparallel to the in-plane direction of light propagation (x in Fig.3a). In Fig.3b the

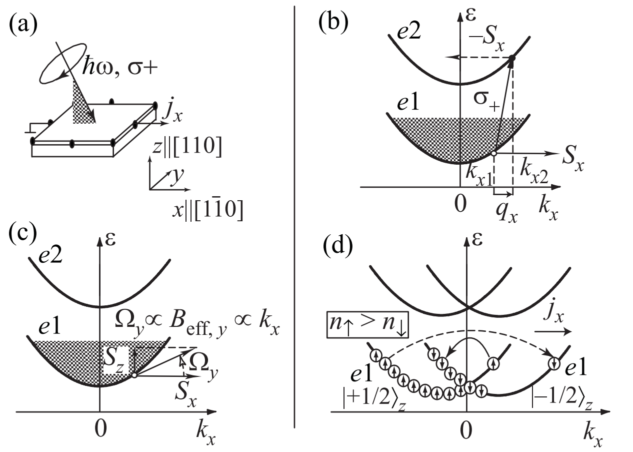

Fig.3. (a) Geometry of the experiment. (b)-(d) Sketch of three sequential stages of the microscopical model of the circular photon drag effect: (b) helicity and photon wave vector dependent photoexcitation, (c) spin rotation in an effective magnetic field caused by spin-orbit coupling, and (d) asymmetrical spin relaxation resulting in an electric current flow due to the spin-galvanic effect

dominating optical transitions are sketched by an inclined arrow to take into account the linear momentum of the photon involved. As a result of the linear momentum transfer the optical transitions occur at a distinct initial electron wave vector determined by energy and momentum conservation. The angular momenta of photons yield a spin polarization S_x at k_{x1} and $-S_x$ at k_{x2} in the subbands $e1$ and $e2$, respectively. These spin polarizations are indicated in Fig.3b by solid and dashed horizontal arrows. While optical excitation results in a spin polarization at well determined wave vectors, k_{x1} in the subband $e1$ and k_{x2} in $e2$, the electrons in the upper subband have sufficient energy to emit optical phonons and rapidly relax due to this process. Thus, the spin polarization S_x in the lower subband only is connected with electrons with the well defined momentum (k_{x1} in Fig.3b).

The second stage is spin precession in an effective magnetic field caused by the Rashba or the Dresselhaus spin-orbit coupling. The orientation and the strength of this effective magnetic field is determined by the direction and the magnitude of the electron wave vector. As our optical excitation results in the spin polarization S_x of electrons with the certain wave vector k_{x1}, the effective magnetic field linked to this wave vector acts on the electron spin. Spins of the electrons, directed just after photoexcitation along the x axis, precess in the effective magnetic field which has both $\Omega_z \propto k_x$ and $\Omega_y \propto k_x$ components. As a consequence of the precession the spin components S_y and S_z appear, see Fig.3c for component S_z. Under steady-state excitation the generation rates of the spin components S_y and S_z are determined by the average angle of spin rotation in the effective magnetic field.

In the third stage, the nonequilibrium spin polarization S_z obtained in the first two stages of the proposed model description drives an electric current. This is due to the spin-galvanic effect caused by asymmetric spin relaxation [5]. The mechanism is briefly sketched in Fig.3d where we, like in the inset of Fig.1a, take into account the spin-orbit splitting of the subbands due to $\sigma_z k_x$-terms in the effective Hamiltonian. The difference in carrier populations in the spin branches $s_z = \pm 1/2$ of the ground subband ($n_\uparrow > n_\downarrow$) causes spin relaxation. The rate of spin-flip scattering depends on the electron wave vectors in the initial and final states that is illustrated by bent arrows of different thicknesses. The transitions of different rates lead to an asymmetric distribution of electrons within each spin branch. As a result an electric current j_x arises. The symmetry analysis shows that the relaxation of the spin component S_y is also accompanied by generation of an electric current along the x direction.

The process of the third stage, spin-galvanic effect, was already studied in [5, 12, 19]. Therefore, we concentrate below on the first two stages and consider them as a specific kind of optical orientation of electron spins, which is caused by simultaneous transfer of photon linear and angular momenta to the carriers.

The intersubband light absorption in n-doped QW structures is a resonant process and possible if the photon energy equals the energy spacing between the subbands. In the single-band approximation, direct optical transitions from the subband $e1$ to the subband $e2$ conserve spin orientation and can be induced only under oblique incidence of the light with nonzero p component of polarization. These selection rules are violated if one takes into account $\mathbf{k}\cdot\mathbf{p}$ admixture of the valence-band states to the conduction-band wave functions. In this model the light of both s- and p-polarization can induce intersubband optical transitions, and the transitions become spin dependent [13, 18]. We assume that electrons occupy the ground subband $e1$ and the size-quantization energy is substantially larger than the mean kinetic energy in the QW plane. Then, the spin matrix of electron photogeneration in the subband $e1$ has the form

$$G_{\mathbf{k}} = -\frac{2\pi}{\hbar} M^\dagger M f_{\mathbf{k}}\, \delta(\hbar\omega + \varepsilon_{1,\mathbf{k}} - \varepsilon_{2,\mathbf{k}+\mathbf{q}_\parallel})\,, \quad (5)$$

where M is a 2×2 matrix describing the intersubband optical transitions, $M^\dagger$ is the hermitian conjugate matrix, $f_{\mathbf{k}}$ is the function of equilibrium carrier distribution, $\varepsilon_{1,\mathbf{k}} = \hbar^2 k^2/2m^*$ and $\varepsilon_{2,\mathbf{k}} = \varepsilon_{21} + \hbar^2 k^2/2m^*$ are the electron dispersions in the subbands $e1$ and $e2$, respectively, m^* is the effective electron mass, ε_{21} is the energy spacing between the subbands, and $\mathbf{q}_\parallel$ is the in-plane component of the photon wave vector. The δ-function in Eq. (5) reflects the resonant behavior of the intersubband optical transitions. In real QW structures the spectral width of the resonance is broadened due to finite scattering time of carriers, fluctuations of the QW width, etc. To describe the broadening one can replace the δ-function by a normalized function δ_Γ which corresponds to the absorption spectrum in the real structure. To first order in the $\mathbf{k}\cdot\mathbf{p}$ theory, the matrix M is given by [18]

$$M = -\frac{eA}{cm^*}\, p_{21} \begin{bmatrix} e_z & \Lambda(e_x - ie_y) \\ -\Lambda(e_x + ie_y) & e_z \end{bmatrix}, \quad (6)$$

where A is the amplitude of the electro-magnetic wave related to the light intensity by $I = A^2\omega^2 n_\omega/(2\pi c)$, c is the light velocity, and p_{21} is the momentum matrix element between the envelope functions of size quantization $\varphi_1(z)$ and $\varphi_2(z)$ in the subbands $e1$ and $e2$,

$$p_{21} = -i\hbar \int \varphi_2(z) \frac{\partial}{\partial z} \varphi_1(z)\, dz. \qquad (7)$$

The parameter Λ originates from $\mathbf{k}\cdot\mathbf{p}$ admixture of valence-band states to the electron wave function and is given by

$$\Lambda = \frac{\varepsilon_{21}\Delta(2E_g + \Delta)}{2E_g(E_g + \Delta)(3E_g + 2\Delta)}\,, \qquad (8)$$

where E_g is the energy of the band gap, and Δ is the energy of spin-orbit splitting of the valence band.

Absorption of circularly polarized light leads to spin orientation of photoexcited carriers. We assume that the momentum relaxation time τ_{e1} is shorter than the precession period in the effective magnetic field, $\Omega\tau_{e1} \ll 1$. Then, the spin generation rate in the subband $e1$ has the form [20]

$$\dot{\mathbf{S}} = \sum_{\mathbf{k}} \mathbf{g}_{\mathbf{k}} + \sum_{\mathbf{k}} \tau_{e1} [\mathbf{\Omega} \times \mathbf{g}_{\mathbf{k}}]\,, \qquad (9)$$

where $\mathbf{g}_{\mathbf{k}} = \mathrm{Tr}(\boldsymbol{\sigma} G_{\mathbf{k}})/2$ is the rate of spin photogeneration into states with the wave vector $\mathbf{k}$, $\boldsymbol{\sigma}$ is the vector of the Pauli matrices. The first term in Eq. (9) describes optical orientation of carriers in the moment of photoexcitation, while the second term stands for spin orientation, which is caused by spin dependent asymmetry of excitation in $\mathbf{k}$-space followed by spin precession in the effective magnetic field. It is the term that describes optical orientation by circularly polarized light, which is related to the transfer of photon linear momenta to charge carriers and vanishes if $\mathbf{q}_{\|} = 0$.

In asymmetrically (110)-grown QW structures the Larmor frequency corresponding to the effective magnetic field has the form

$$\mathbf{\Omega} = \frac{2}{\hbar}(\beta_{xy} k_y,\, \beta_{yx} k_x,\, \beta_{zx} k_x), \qquad (10)$$

where β_{xy}, β_{yx} and β_{zx} are constants of the spin-orbit interaction. As in the experiment described above, we consider that the light wave vector $\mathbf{q}$ lies in the xz plane. Then, for the Boltzmann distribution of carriers, one derives

$$\dot{S}_x = \Lambda \eta_z(\hbar\omega) \frac{q_x}{2q} \frac{I P_{\mathrm{circ}}}{\hbar\omega}, \qquad (11)$$

$$\dot{S}_y = -q_x\, \bar{\varepsilon}\, \Lambda \frac{\beta_{zx}\tau_{e1}}{\hbar} \frac{q_x}{q} \frac{d\,\eta_z(\hbar\omega)}{d\,\hbar\omega} \frac{I P_{circ}}{\hbar\omega}, \qquad (12)$$

$$\dot{S}_z = \left[\eta_z(\hbar\omega)\Lambda^2 \frac{q_z}{2q} + q_x \bar{\varepsilon}\, \Lambda \frac{\beta_{yx}\tau_{e1}}{\hbar} \frac{q_x}{q} \frac{d\,\eta_z(\hbar\omega)}{d\,\hbar\omega} \right] \frac{I P_{circ}}{\hbar\omega}, \qquad (13)$$

where $\bar{\varepsilon} = k_B T$ is the mean kinetic energy of equilibrium carriers, T is the temperature, $\eta_z(\hbar\omega)$ is the QW absorbance for light polarized along the growth direction,

$$\eta_z(\hbar\omega) = \frac{4\pi^2\alpha}{n_\omega} \frac{\hbar |p_{21}|^2}{m^{*2}\omega}\, n_s\, \delta_\Gamma(\hbar\omega - \varepsilon_{21}), \qquad (14)$$

and α is the fine-structure constant.

As addressed above, relaxation of spin components S_y and S_z in (110)-oriented QW structures is accompanied by the generation of an electric current along the x axis due to the spin-galvanic effect. Equations (12) and (13) show that spin components S_y and S_z contain contributions proportional to the photon wave vector q_x and the light helicity P_{circ}. Therefore, the generated photocurrent can be gathered in a class of photon drag effects denoted as the circular photon drag effect.

4. Conclusion. We have studied spin dependent photocurrents in n-doped zinc-blende-based (110)-grown QWs caused by direct intersubband transitions induced by infrared radiation and the Drude absorption of terahertz radiation. The helicity dependent photocurrent observed at normal incidence of the infrared radiation is mostly due to the circular photogalvanic effect. Under oblique incidence, however, the helicity dependent photocurrent at large angles of incidence flows in the direction opposite to that excited at normal incidence. We demonstrated that the inversion of the current sign is a result of the interplay between the circular photogalvanic effect and the circular photon drag effect. Microscopic theory of the latter effect developed in the present work is based on optical spin orientation sensitive to the photon wave vector and subsequent asymmetric spin relaxation.

We are grateful to E.L. Ivchenko and V.V. Bel'kov for helpful discussions and thank I. Gronwald for technical assistance. This work was supported by the Deutsche Forschungsgemeinschaft through SFB 689 and GRK638, the RFBR, programs of the RAS and Russian Ministry of Education and Science, Russian Science Support Foundation, and Foundation "Dynasty"-ICFPM.

1. Y. Ohno, R. Terauchi, T. Adachi et al., Phys. Rev. Lett. **83**, 4196 (1999).
2. S.D. Ganichev, E.L. Ivchenko, S.N. Danilov et al., Phys. Rev. Lett. **86**, 4358 (2001).
3. M. Bieler, N. Laman, H.M. van Driel, and A.L. Smirl, Appl. Phys. Lett. **86**, 061102 (2005).
4. C.L. Yang, H.T. He, Lu Ding et al., Phys. Rev. Lett. **96**, 186605 (2006).

5. S. D. Ganichev, E. L. Ivchenko, V. V. Bel'kov et al., Nature (London) **417**, 153 (2002).
6. S. D. Ganichev and W. Prettl, *Intense Terahertz Excitation of Semiconductors*, Oxford University Press, Oxford, 2006.
7. B. I. Sturman and V. M. Fridkin, *The photogalvanic effect and relative phenomena in non-centrosymmetric media* (in Russian), M.: Nauka, 1992 [English translation: *The Photovoltaic and Photorefractive Effects in Non-Centrosymmetric Materials*, Gordon and Breach Science Publishers, New York, 1992].
8. E. L. Ivchenko and G. E. Pikus, in *Problems of Modern Physics* (in Russian), Eds. V. M. Tuchkevich and V. Ya. Frenkel, Nauka, Leningrad, 1980, p. 275 [English translation: *Semiconductor Physics*, Eds. V. M. Tuchkevich and V. Ya. Frenkel, Cons. Bureau, New York, 1986, p. 427].
9. V. I. Belinicher, Fiz. Tverd. Tela **23**, 3461 (1981) [Sov. Phys. Solid State **23**, 2012 (1981)].
10. I. D. Yaroshetskii and S. M. Ryvkin, in *Problems of Modern Physics* (in Russian), Eds. V. M. Tuchkevich and V. Ya. Frenkel, Nauka, Leningrad, 1980, p. 173 [English translation: *Semiconductor Physics*, Eds. V. M. Tuchkevich and V. Ya. Frenkel, Cons. Bureau, New York, 1986, p. 249].
11. A. F. Gibson and M. F. Kimmitt, in *Infrared and Millimeter Waves*, Vol. 3, *Detection of Radiation*, Ed. K. J. Button, Academic Press, New York, 1980, p. 181.
12. S. D. Ganichev, Petra Schneider, V. V. Bel'kov et al., Phys. Rev. B. **68**, 081302 (2003).
13. S. D. Ganichev, V. V. Bel'kov, Petra Schneider et al., Phys. Rev. B **68**, 035319 (2003).
14. L. I. Magarill and M. V. Entin, Poverkhnost' **1**, 74 (1982) [in Russian].
15. G. M. Gusev, Z. D. Kvon, L. I. Magarill et al., Pis'ma Zh. Eksp. Teor. Fiz. **46**, 28 (1987) [Sov. JETP Lett. **46**, 33 (1987)].
16. S. Luryi, Phys. Rev. Lett. **58**, 2263 (1987).
17. A. D. Wieck, H. Sigg, and K. Ploog, Phys. Rev. Lett. **64**, 463 (1990).
18. E. L. Ivchenko and S. A. Tarasenko, Zh. Eksp. Teor. Fiz. **126**, 426 (2004) [JETP **99**, 379 (2004)].
19. E. L. Ivchenko, Yu. B. Lyanda-Geller, and G. E. Pikus, Zh. Eksp. Teor. Fiz. **98**, 989 (1990) [Sov. Phys. JETP **71**, 550 (1990)].
20. S. A. Tarasenko, Phys. Rev. B **72**, 113302 (2005).